Journal of Materials Chemistry C



PAPER

View Article Online

View Journal | View Issue



Cite this: *J. Mater. Chem. C*, 2018, **6**, 66

Received 4th October 2017, Accepted 28th November 2017

DOI: 10.1039/c7tc04520d

rsc.li/materials-c

Enhancing the performance of a fused-ring electron acceptor *via* extending benzene to naphthalene†

Jingshuai Zhu,^{ab} Yang Wu,^c Jeromy Rech, ^o Jiayu Wang,^b Kuan Liu,^b Tengfei Li,^b Yuze Lin,*^{ae} Wei Ma,^c Wei You ^o and Xiaowei Zhan ^o*

We compared an indacenodithiophene(IDT)-based fused-ring electron acceptor IDIC1 with its counterpart IHIC1 in which the central benzene unit is replaced by a naphthalene unit, and investigated the effects of the benzene/naphthalene core on the optical and electronic properties as well as on the performance of organic solar cells (OSCs). Compared with benzene-cored IDIC1, naphthalene-cored IHIC1 shows a larger π -conjugation with stronger intermolecular π - π stacking. Relative to benzene-cored IDIC1, naphthalene-cored IHIC1 shows a higher lowest unoccupied molecular orbital energy level (IHIC1: -3.75 eV, IDIC1: -3.81 eV) and a higher electron mobility (IHIC1: 3.0×10^{-4} cm² V⁻¹ s⁻¹, IDIC1: 1.5×10^{-4} cm² V⁻¹ s⁻¹). When paired with the polymer donor FTAZ that has matched energy levels and a complementary absorption spectrum, IHIC1-based OSCs show higher values of open-circuit voltage, short-circuit current density, fill factor and power conversion efficiency relative to those of the IDIC1-based control devices. These results demonstrate that extending benzene in IDT to naphthalene is a promising approach to upshift energy levels, enhance electron mobility, and finally achieve higher efficiency in nonfullerene acceptor-based OSCs.

Introduction

Solution-processed bulk heterojunction (BHJ) organic solar cells (OSCs) are a cost-effective alternative for utilizing solar energy, and possess some advantages, such as light weight, low cost and flexibility. Fullerene derivatives, such as $PC_{61}BM$ and $PC_{71}BM$, are widely used electron acceptors in OSCs since they have high electron affinity, isotropic charge transport and high electron mobility. However, the deficiencies of fullerene acceptor materials, such as difficult chemical modification, limited energy level variability, weak absorption in the visible region, and morphology instability in a BHJ, hinder the further

development of OSCs. ^{10,11} Therefore, it is necessary to develop nonfullerene acceptors. Compared with fullerene acceptors, the chemical structure and the electronic and optical properties of nonfullerene acceptors are readily tuned. ^{12–15}

Recently, we reported the original fused-ring electron acceptors (FREAs) with an acceptor–donor–acceptor structure based on indacenodithiophene (IDT) or indacenodithienothiophene (IDTT) end-capped with 1,1-dicyanomethylene-3-indanone, exemplified by the star molecule ITIC. ¹⁶ The rigid extended fused-ring structure of IDT and IDTT prevents rotational disorder, reduces reorganization energy, and exhibits suitable lowest unoccupied molecular orbital (LUMO) and highest occupied molecular orbital (HOMO) energy levels, broad and strong absorption, and relatively high electron mobility. ^{17–19} OSCs based on these FREAs exhibit high power conversion efficiencies (PCEs) with good device stability. ^{20–32}

The naphthalene ring shows larger π -conjugation than the benzene ring, and integration of naphthalene into a rigid and coplanar backbone may facilitate π -electron delocalization, reduce energetic disorder and induce strong intermolecular interactions for efficient charge transport. A few naphthalene-based nonfullerene acceptors were reported and exhibited promising performance in OSCs with PCEs of 8–9%. However, there is no work to compare naphthalene- and benzene-cored nonfullerene acceptors and probe how naphthalene

^a Department of Chemistry, Capital Normal University, Beijing 100048, China. E-mail: linyz@iccas.ac.cn

b Department of Materials Science and Engineering, Key Laboratory of Polymer Chemistry and Physics of Ministry of Education, College of Engineering, Peking University, Beijing 100871, China. E-mail: xwzhan@pku.edu.cn

^c State Key Laboratory for Mechanical Behavior of Materials, Xi'an Jiaotong University, Xi'an 710049, China

^d Department of Chemistry, University of North Carolina at Chapel Hill, North Carolina 27599, USA

^e Department of Applied Physical Sciences, University of North Carolina at Chapel Hill, North Carolina 27599, USA

[†] Electronic supplementary information (ESI) available: CV curves, absorption spectra, SCLC measurements, AFM images, TEM images, GIWAXS, OSC data. See DOI: 10.1039/c7tc04520d

Chart 1 Chemical structures of FTAZ, IDIC1 and IHIC1.

and benzene differ in affecting the performance of nonfullerene acceptors.

In this work, we synthesized a FREA based on the naphthalene ring as a core (IHIC1, Chart 1), which was published when we prepared this paper,³⁸ compared with its counterpart based on the benzene core (IDIC1, Chart 1) reported in our previous work, and investigated how naphthalene and benzene affect the FREA performance. In comparison with benzene-cored IDIC1, naphthalene-cored IHIC1 exhibits upshifted HOMO and LUMO energy levels and enhanced electron mobility. Furthermore, as-cast OSCs based on blends of IHIC1 and a wide-bandgap polymer donor FTAZ⁴⁰ (Chart 1) exhibit a PCE of 9.21%, higher than that of IDIC1-based OSCs (7.13%).

Results and discussion

Optical and electronic properties

The HOMO and LUMO energies of the IDIC1 film are estimated to be -5.51 eV and -3.81 eV from the onset oxidation and reduction potentials (Fig. S1a, ESI†), respectively. IHIC1 shows higher energy levels (HOMO = -5.47 eV; LUMO = -3.75 eV) relative to IDIC1 (Fig. 1a). The higher LUMO energy level of IHIC1 is beneficial to high open-circuit voltage $(V_{\rm OC})$ in OSCs. In solution, IDIC1 and IHIC1 exhibit maximum absorption peaks at 656 nm and 651 nm, respectively (Fig. S1b, ESI†). In the thin film, IDIC1 and IHIC1 show maximum absorption

peaks at 686 nm and 674 nm, respectively. Relative to IDIC1, IHIC1 exhibits slightly blue-shifted absorption. The optical bandgaps of IDIC1 and IHIC1 films are 1.67 eV and 1.69 eV, estimated from the absorption edge at 743 nm and 732 nm, respectively (Fig. 1b). The electron mobilities of IDIC1 and IHIC1 films, measured using the space-charge-limited current (SCLC) method, are 1.5×10^{-4} and 3.0×10^{-4} cm² V⁻¹ s⁻¹, respectively (Fig. S2, ESI†).

Photovoltaic properties

In our previous work, we reported a wide-bandgap polymer donor FTAZ. 40 FTAZ exhibits strong absorption at 400-620 nm, which complements those of IDIC1 and IHIC1 at 500-750 nm. Energy levels of FTAZ (HOMO = -5.38 eV; LUMO = -3.17 eV) match with those of IDIC1 and IHIC1. Thus, we used FTAZ as a donor and IDIC1 or IHIC1 as an acceptor to fabricate OSCs with a structure of indium tin oxide (ITO)/ZnO/FTAZ:IDIC1(or IHIC1)/MoO₃/Ag. The optimized donor: acceptor (D/A) weight ratio is 1:1.5 (Table S1, ESI \dagger). Table 1 summarizes V_{OC} , shortcircuit current density (J_{SC}) , fill factor (FF) and PCE of the optimized devices. OSCs based on the as-cast FTAZ: IHIC1 (1:1.5, w/w) film give a V_{OC} of 0.950 V, a J_{SC} of 14.3 mA cm⁻², a FF of 67.9% and a PCE of 9.21%, while OSCs based on the as-cast FTAZ: IDIC1 (1:1.5, w/w) film give a V_{OC} of 0.896 V, a J_{SC} of 13.6 mA cm $^{-2}$, a FF of 58.5% and a PCE of 7.13% (Fig. 2a). Compared with the FTAZ:IDIC1 system, FTAZ:IHIC1-based

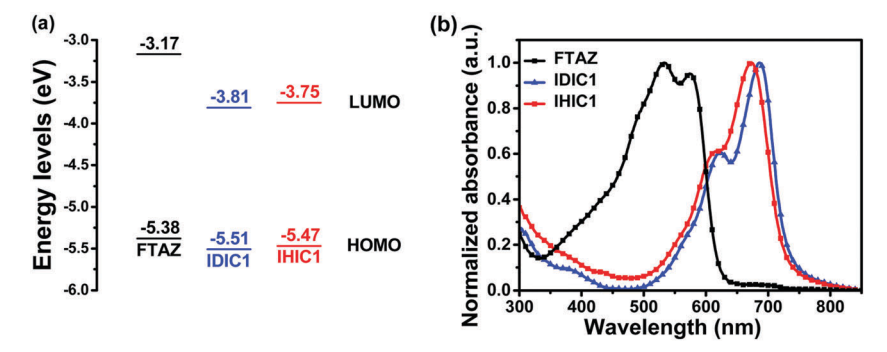


Fig. 1 (a) Energy levels of FTAZ, IDIC1 and IHIC1 calculated from cyclic voltammetry. (b) UV-vis absorption spectra of FTAZ, IDIC1 and IHIC1 in a thin film.

Table 1 Device data of OSCs under the illumination of AM 1.5 G, 100 mW cm⁻² (average data are obtained from 20 devices, best data in brackets)

Active layers	$V_{\mathrm{OC}}\left(\mathrm{V}\right)$	$J_{ m SC}~({ m mA~cm}^{-2})$	FF (%)	PCE (%)	Calculated $J_{\rm SC}$ (mA cm $^{-2}$)
FTAZ:IDIC1	$0.894 \pm 0.005 (0.896)$	$13.5 \pm 0.1 (13.6)$	$58.1 \pm 1.2 (58.5)$	$7.05 \pm 0.17 (7.13)$	13.2
FTAZ:IHIC1	$0.947 \pm 0.005 (0.950)$	$14.2 \pm 0.2 (14.3)$	$66.4 \pm 0.6 (67.9)$	$8.91 \pm 0.16 \ (9.21)$	13.8

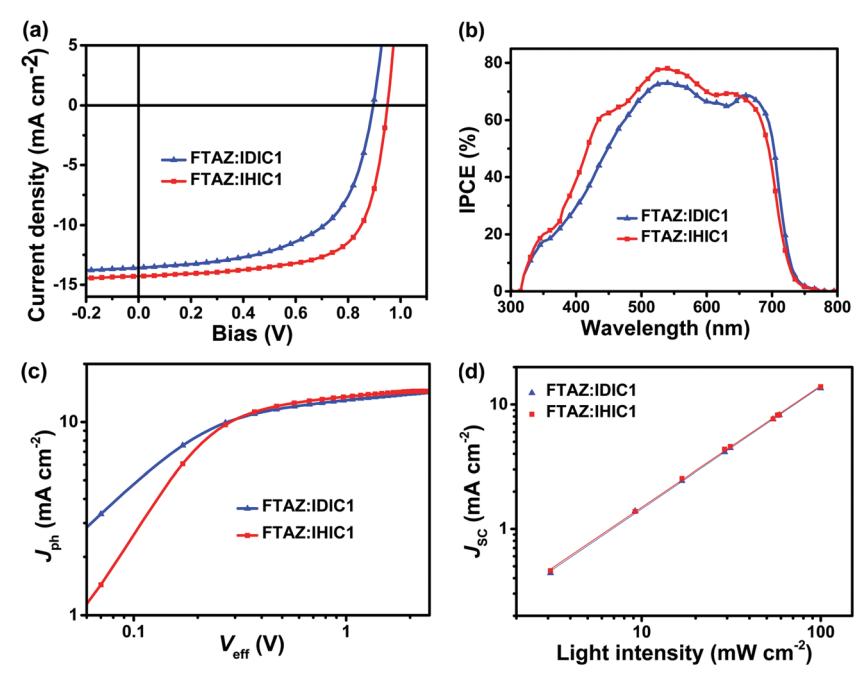


Fig. 2 (a) J-V curves, (b) IPCE spectra, (c) J_{ph} versus V_{eff} characteristics, and (d) J versus light intensity of devices with the structure ITO/ZnO/active layer/MoO₃/Ag.

devices show a higher $V_{\rm OC}$, a higher $J_{\rm SC}$ and a higher FF. The higher $V_{\rm OC}$ is related to the higher LUMO level of IHIC1.

The incident photon to converted current efficiency (IPCE) spectra of the optimized devices are shown in Fig. 2b. The OSCs based on FTAZ:IDIC1 and FTAZ:IHIC1 show a broad photoresponse from 300 to 750 nm. The IPCE of FTAZ:IHIC1 based devices is higher than that of FTAZ:IDIC1 based devices at 300–650 nm. The IPCE of FTAZ:IDIC1 based devices red shifts relative to that of FTAZ:IHIC1 based devices at 650–750 nm, due to red-shifted absorption of IDIC. The maximum IPCEs of FTAZ:IDIC1 and FTAZ:IHIC1 are 72.92% and 76.83%, respectively. The $J_{\rm SC}$ values of FTAZ:IDIC1 and FTAZ:IHIC1-based devices calculated from the integration of the IPCE spectra with the AM 1.5G reference spectrum are 13.2 and 13.8 mA cm⁻², respectively, which is in good agreement with $J_{\rm SC}$ measured from J-V (the error is <5%).

To probe the exciton/charge dynamics, we measured the photocurrent density $(J_{\rm ph})$ versus the effective voltage $(V_{\rm eff})$ to study the charge generation, dissociation and extraction properties. In Fig. 2c, at a high applied voltage $(V_{\rm eff}>2~{\rm V})$, $J_{\rm ph}$ reaches saturation, implying that almost all excitons are dissociated and photo-generated charge carriers are completely collected by the electrodes. The charge dissociation probability can be calculated from $J_{\rm SC}/J_{\rm sat}$. The $J_{\rm ph}/J_{\rm sat}$ ratios for the devices of FTAZ:IDIC1 and FTAZ:IHIC1 is calculated to be 95.8% and 96.7% under the short circuit conditions, respectively, indicating efficient charge dissociation and collection.

To gain insights into charge recombination in the active layer, light intensity dependent photocurrent measurement was carried out for the optimized device. $J_{\rm SC}$ follows a power-law dependence on incident light intensity ($P_{\rm light}$): $J_{\rm SC} \propto P_{\rm light}^{\alpha}$ (Fig. 2d).⁴² For extreme conditions, α is equal to 0.75 when space charge buildup reaches a fundamental limit; α is equal to 1

when no space charge exists. The α values of FTAZ:IDIC1 and FTAZ:IHIC1 are 0.983 and 0.978, respectively, suggesting negligible bimolecular charge recombination under the short circuit conditions.

The SCLC method was employed to measure the hole mobility and electron mobility of FTAZ:IDIC1 and FTAZ:HIC1 blended films (Fig. S3, ESI†). The as-cast blended film of FTAZ:IDIC1 exhibits a hole mobility (μ_h) of 1.3×10^{-4} cm² V⁻¹ s⁻¹ and an electron mobility (μ_e) of 2.0×10^{-5} cm² V⁻¹ s⁻¹ with a μ_h/μ_e ratio of 6.5, while the as-cast blended film of FTAZ:IHIC1 exhibits a μ_h of 1.5×10^{-4} cm² V⁻¹ s⁻¹ and a μ_e of 2.6×10^{-5} cm² V⁻¹ s⁻¹ with a μ_h/μ_e ratio of 5.8. The higher and more balanced charge mobilities of the FTAZ:IHIC1 blend are responsible for the higher J_{SC} and the higher FF of the device.

Film morphology

The morphology of the blended films of FTAZ:IDIC1 and FTAZ: IHIC1 is studied by atomic force microscopy (AFM), transmission electron microscopy (TEM), grazing-incidence wide-angle X-ray scattering (GIWAXS) and Resonant soft X-ray scattering (R-SoXS). We used AFM to characterize the surface morphology of active layers (Fig. S4, ESI†). Both FTAZ:IDIC1 and FTAZ:IHIC1 films have a smooth and uniform surface. The root-mean-square roughness values of FTAZ:IDIC1 and FTAZ:IHIC1 films are 0.64 nm and 0.95 nm, respectively. In the TEM images (Fig. S5, ESI†), the blended film of FTAZ:IDIC1 shows low contrast, while the FTAZ:IHIC1 blended film shows visible contrast, which is consistent with the AFM images, suggesting the stronger crystallinity of the FTAZ:IHIC1 film. The GIWAXS measurement was used to probe the molecular packing of FTAZ:IDIC1 and FTAZ: IHIC1 blended films (Fig. 3).⁴³ The peak at $q \approx 0.34 \text{ Å}^{-1}$ is generated from the lamellar packing of FTAZ. The π - π stacking

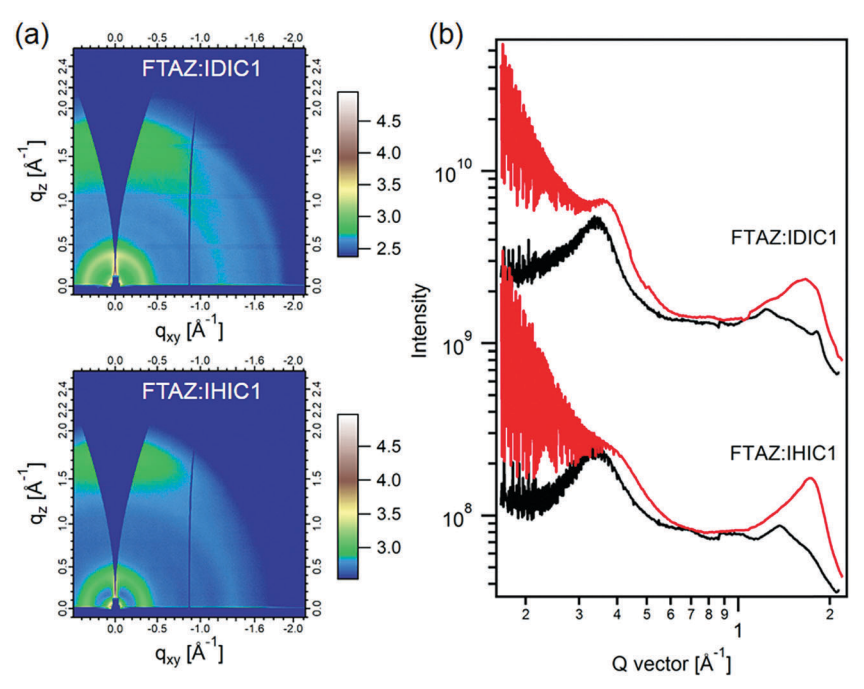


Fig. 3 (a) 2D GIWAXS patterns and (b) scattering profiles of in-plane and out-of-plane for blended films

peaks of FTAZ, IDIC1 and IHIC1 are located at $q \approx 1.67$, 1.82 and 1.78 Å^{-1} , respectively. The scattering profiles of the corresponding neat films are shown in Fig. S6 (ESI†). IHIC1 shows stronger π - π stacking than IDIC1 in the as-cast films. The coherence length of π - π stacking for IDIC1 and IHIC1 in blended films is calculated to be 1.9 and 2.2 nm, respectively. The enhanced π - π stacking of IHIC1 is beneficial to the charge transport, leading to higher electron mobility in neat and blended films. The phase separation of FTAZ:IDIC1 and FTAZ: IHIC1 blended films was investigated by R-SoXS (Fig. 4).44 The photon energy of 285.2 eV was selected to provide enhanced

FTAZ: IDIC1 FTAZ: IHIC1 ntensity·q² (a.u.)

Fig. 4 R-SoXS profiles in log scale for FTAZ:IDIC1 and FTAZ:IHIC1 blended films.

q (nm⁻¹)

material contrasts. Both blended films exhibit a scattering peak at $\sim 0.25 \text{ nm}^{-1}$, corresponding to the characterized length scale of ~ 25 nm. These length scales are close to the diffusion length of exciton, thus are favorable for charge separation. Furthermore, the total scattering intensity (TSI, calculated by integrating the scattering profiles) can be used to describe the relative domain purity of the blended films. The higher the TSI, the purer the domains. The relative domain purity of FTAZ: IDIC1 and FTAZ:IHIC1 blend films is the same (88%).

Conclusions

In summary, we compared benzene-cored (IDIC1) and naphthalenecored (IHIC1) FREAs and investigated the effects of the benzene/ naphthalene unit on the optical and electronic properties as well as on the performance of OSCs. Compared with benzene-cored IDIC1, naphthalene-cored IHIC1 shows a larger π -conjugation with stronger intermolecular π - π stacking. Thus, IHIC1 has upshifted energy levels and higher electron mobility. When paired with the polymer donor FTAZ that has matched energy levels and a complementary absorption spectrum, the IHIC1-based OSCs show higher values of $V_{\rm OC}$, $I_{\rm SC}$ and FF. The as-cast OSCs based on FTAZ:IHIC1 without any additional treatment yield PCEs of up to 9.21%, much higher than that of the control devices based on FTAZ:IDIC1 (7.13%). The higher $V_{\rm OC}$ in FTAZ:IHIC1-based devices is attributed to the higher LUMO level of IHIC1 in comparison with IDIC1. The FTAZ:IHIC1-based devices show better and balanced charge transport, contributing to the higher J_{SC} and higher FF. These results demonstrate that extending benzene in the electron-donating fused-ring IDT unit to naphthalene is a promising approach to upshift energy levels, enhance electron mobility, and finally achieve higher efficiency in FREA-based OSCs.

Experimental section

Materials

Unless stated otherwise, all chemical reagents and solvents used were obtained commercially and were used without further purification. IDIC1,¹³ IHIC1³⁸ and FTAZ⁴⁰ were synthesized according to the literature procedure.

Measurements

Solution (chloroform) and thin film (on quartz substrate) UV-vis absorption spectra were recorded using a JASCO V-570 spectrophotometer. Electrochemical measurements were carried out under nitrogen in a solution of tetra-n-butylammonium hexafluorophosphate ($[^nBu_4N]^+[PF_6]^-$) (0.1 M) in CH₃CN employing a computer-controlled CHI660C electrochemical workstation, a glassy carbon working electrode coated with IDIC1 and IHIC1 films, an Ag/AgCl reference electrode, and a platinum-wire auxiliary electrode. The potentials were referenced to a ferrocenium/ferrocene (FeCp₂^{+/0}) couple using ferrocene as an internal standard. The transmission electron microscopy (TEM) characterization was carried out on a JEM-2100 transmission electron microscope operated at 200 kV. The samples for the TEM measurements were prepared as follows: the active layer films were spin-casted on ITO/poly(3,4-ethylenedioxythiophene):poly(styrene sulfonate) (PEDOT:PSS) substrates, and the substrates with the active layers were submerged in deionized water to make the active layers float at the air-water interface. Then, the floated films were picked up on unsupported 200 mesh copper grids for the TEM measurements. The nanoscale morphology of the blends was observed using a Multimode 8 scanning probe microscope (Bruker) in the tapping mode.

GIWAXS measurements were performed at beamline 7.3.3 at the Advanced Light Source (ALS). Samples were prepared on Si substrates using identical blend solutions as used in OSC devices. The 10 keV X-ray beam was incident at a grazing angle of 0.11-0.15°, which maximized the scattering intensity from the samples. The scattered X-rays were detected using a Dectris Pilatus 2 M photon counting detector. R-SoXS transmission measurements were performed at beamline 11.0.1.2 at the ALS. Samples for R-SoXS measurements were prepared on a PEDOT: PSS modified Si substrate under the same conditions as used for the OSC device fabrication, and then transferred by floating in water to a 1.5 mm \times 1.5 mm, 100 nm thick Si₃N₄ membrane supported by a 5 mm \times 5 mm, 200 mm thick Si frame (Norcada Inc.). Two dimensional scattering patterns were collected on an in-vacuum CCD camera (Princeton Instrument PI-MTE). The beam size at the sample is 100 μ m \times 200 μ m. The composition variation (or relative domain purity) over the length scales probed can be extracted by integrating scattering profiles to yield the total scattering intensity.

Fabrication and characterization of OSCs

OSCs were fabricated with the structure of ITO/ZnO/FTAZ: acceptor/MoO $_3$ /Ag. The patterned ITO glass (sheet resistance = 10 Ω \square ⁻¹) was pre-cleaned in an ultrasonic bath with acetone and isopropanol. The ZnO electron transport layer was prepared

onto the ITO glass through spin coating at 4000 rpm from a ZnO precursor solution, then the ZnO substrates were immediately baked in air at 200 °C for 30 min. A CHCl₃ solution (totally 12.5 mg mL⁻¹) of the FTAZ:acceptor was spin-coated (3000 rpm) on the ZnO layer to form a photoactive layer (ca. 100 nm). The thickness of the photoactive layer was measured using a Bruker Dektak-XT. The MoO₃ layer (ca. 5 nm) and Ag (ca. 80 nm) were successively evaporated onto the surface of the photoactive layer under vacuum (ca. 10^{-5} Pa). The active area of the device was ca. 4 mm². An XES-70S1 (SAN-EI Electric Co., Ltd) solar simulator (AAA grade, $70 \times 70 \text{ mm}^2$ photobeam size) coupled with AM 1.5G solar spectrum filters was used as the light source, and the optical power at the sample was 100 mW cm⁻². A 2 \times 2 cm² monocrystalline silicon reference cell (SRC-1000-TC-QZ) was purchased from VLSI Standards Inc. The current-voltage (J-V) measurement of the devices was conducted using a computercontrolled Agilent B2912A Precision Source/Measure Unit (Agilent Technologies). The IPCE spectrum was measured using a Solar Cell Spectral Response Measurement System QE-R3011 (Enlitech Co., Ltd). The light intensity at each wavelength was calibrated using a standard single crystal Si photovoltaic cell.

Mobility measurements

Hole-only or electron-only diodes were fabricated using the architectures: ITO/PEDOT:PSS/FTAZ:acceptor/Au for holes and Al/FTAZ:acceptor/Al or Al/acceptor/Al for electrons. A chloroform solution (totally 12.5 mg mL⁻¹) of the acceptor or the FTAZ: acceptor (1:1.5, w/w) was spin-coated (3000 rpm). Mobilities were extracted by fitting the current density-voltage curves using space charge limited current (SCLC). The J-V curves of the devices were plotted as $\ln[Jd^3/V^2]$ versus $[V/d]^{0.5}$ using equation $J=9\varepsilon_0\varepsilon_r\mu_h(\mu_e)V^2/8d^3$ for holes and electrons, where J is the current density, d is the film thickness of the active layer (ca. 100 nm), μ_h is the hole mobility, μ_e is the electron mobility, ε_r is the relative dielectric constant of the transport medium, and ε_0 is the permittivity of free space (8.85 × 10⁻¹² F m⁻¹). $V = V_{\rm appl} - V_{\rm bi}$, $V_{\rm appl}$ is the applied voltage and $V_{\rm bi}$ is the offset voltage.

Conflicts of interest

There are no conflicts of interest to declare.

Acknowledgements

X. Z. thanks NSFC (21734001). Y. L. thanks NSFC (21504058) and Scientific Research Project of Beijing Educational Committee (KM201610028006). W. M. thanks NSFC (21504066, 21534003) and the Ministry of Science and Technology of China (2016YFA0200700). W. Y. thanks NSF (DMR-1507249 and CBET-1639429). X-ray data were acquired at beamlines 7.3.3 and 11.0.1.2 at the Advanced Light Source, which is supported by the Director, Office of Science, Office of Basic Energy Sciences, of the U.S. Department of Energy under Contract No. DE-AC02-05CH11231.

Notes and references

- 1 L. Lu, T. Zheng, Q. Wu, A. M. Schneider, D. Zhao and L. Yu, *Chem. Rev.*, 2015, **115**, 12666.
- 2 Y. Lin and X. Zhan, Acc. Chem. Res., 2016, 49, 175.
- 3 F. C. Krebs, N. Espinosa, M. Hösel, R. R. Søndergaard and M. Jørgensen, *Adv. Mater.*, 2014, **26**, 29.
- 4 A. J. Heeger, Adv. Mater., 2014, 26, 10.
- 5 L. Dou, J. You, Z. Hong, Z. Xu, G. Li, R. A. Street and Y. Yang, Adv. Mater., 2013, 25, 6642.
- 6 J. Wang, K. Liu, L. Ma and X. Zhan, Chem. Rev., 2016, 116, 14675.
- 7 G. Yu, J. Gao, J. C. Hummelen, F. Wudl and A. J. Heeger, Science, 1995, 270, 1789.
- 8 C. Z. Li, J. Huang, H. Ju, Y. Zang, J. Zhang, J. Zhu, H. Chen and A. K. Jen, *Adv. Mater.*, 2016, 28, 7269.
- 9 J. Zhao, Y. Li, G. Yang, K. Jiang, H. Lin, H. Ade, W. Ma and H. Yan, *Nat. Energy*, 2016, 1, 15027.
- 10 Y. Lin and X. Zhan, Mater. Horiz., 2014, 1, 470.
- 11 Y. Lin and X. Zhan, Adv. Energy Mater., 2015, 5, 1501063.
- 12 S. Holliday, R. S. Ashraf, A. Wadsworth, D. Baran, S. A. Yousaf, C. B. Nielsen, C. Tan, S. D. Dimitrov, Z. Shang, N. Gasparini, M. Alamoudi, F. Laquai, C. J. Brabec, A. Salleo, J. R. Durrant and I. McCulloch, *Nat. Commun.*, 2016, 7, 11585.
- 13 Y. Lin, T. Li, F. Zhao, L. Han, Z. Wang, Y. Wu, Q. He, J. Wang, L. Huo, Y. Sun, C. Wang, W. Ma and X. Zhan, *Adv. Energy Mater.*, 2016, 6, 1600854.
- 14 Y. Wu, H. Bai, Z. Wang, P. Cheng, S. Zhu, Y. Wang, W. Ma and X. Zhan, *Energy Environ. Sci.*, 2015, **8**, 3215.
- 15 Y. Lin, Q. He, F. Zhao, L. Huo, J. Mai, X. Lu, C.-J. Su, T. Li, J. Wang, J. Zhu, Y. Sun, C. Wang and X. Zhan, *J. Am. Chem. Soc.*, 2016, 138, 2973.
- 16 Y. Lin, J. Wang, Z. G. Zhang, H. Bai, Y. Li, D. Zhu and X. Zhan, *Adv. Mater.*, 2015, 27, 1170.
- 17 F. Liu, Z. Zhou, C. Zhang, T. Vergote, H. Fan, F. Liu and X. Zhu, J. Am. Chem. Soc., 2016, 138, 15523.
- 18 W. Wang, C. Yan, T. K. Lau, J. Wang, K. Liu, Y. Fan, X. Lu and X. Zhan, *Adv. Mater.*, 2017, **29**, 1701308.
- 19 Y. Lin, F. Zhao, Q. He, L. Huo, Y. Wu, T. C. Parker, W. Ma, Y. Sun, C. Wang, D. Zhu, A. J. Heeger, S. R. Marder and X. Zhan, J. Am. Chem. Soc., 2016, 138, 4955.
- 20 F. Zhao, S. Dai, Y. Wu, Q. Zhang, J. Wang, L. Jiang, Q. Ling, Z. Wei, W. Ma, W. You, C. Wang and X. Zhan, *Adv. Mater.*, 2017, 29, 1700144.
- 21 J. Zhu, Z. Ke, Q. Zhang, J. Wang, S. Dai, Y. Wu, Y. Xu, Y. Lin, W. Ma, W. You and X. Zhan, *Adv. Mater.*, 2017, DOI: 10.1002/adma.201704713.
- 22 S. Dai, F. Zhao, Q. Zhang, T. K. Lau, T. Li, K. Liu, Q. Ling, C. Wang, X. Lu, W. You and X. Zhan, *J. Am. Chem. Soc.*, 2017, 139, 1336.
- 23 P. Cheng, M. Zhang, T. K. Lau, Y. Wu, B. Jia, J. Wang, C. Yan, M. Qin, X. Lu and X. Zhan, Adv. Mater., 2017, 29, 1605216.

- 24 Y. Lin, F. Zhao, Y. Wu, K. Chen, Y. Xia, G. Li, S. K. Prasad, J. Zhu, L. Huo, H. Bin, Z. G. Zhang, X. Guo, M. Zhang, Y. Sun, F. Gao, Z. Wei, W. Ma, C. Wang, J. Hodgkiss, Z. Bo, O. Inganas, Y. Li and X. Zhan, Adv. Mater., 2017, 29, 1604155.
- 25 Y. Cui, H. Yao, B. Gao, Y. Qin, S. Zhang, B. Yang, C. He, B. Xu and J. Hou, J. Am. Chem. Soc., 2017, 139, 7302.
- 26 H. Bin, L. Gao, Z. G. Zhang, Y. Yang, Y. Zhang, C. Zhang, S. Chen, L. Xue, C. Yang, M. Xiao and Y. Li, *Nat. Commun.*, 2016, 7, 13651.
- 27 D. Baran, R. S. Ashraf, D. A. Hanifi, M. Abdelsamie, N. Gasparini, J. A. Rohr, S. Holliday, A. Wadsworth, S. Lockett, M. Neophytou, C. J. Emmott, J. Nelson, C. J. Brabec, A. Amassian, A. Salleo, T. Kirchartz, J. R. Durrant and I. McCulloch, *Nat. Mater.*, 2017, 16, 363.
- 28 S. Chen, Y. Liu, L. Zhang, P. C. Y. Chow, Z. Wang, G. Zhang, W. Ma and H. Yan, J. Am. Chem. Soc., 2017, 139, 6298.
- 29 J. Wang, W. Wang, X. Wang, Y. Wu, Q. Zhang, C. Yan, W. Ma, W. You and X. Zhan, *Adv. Mater.*, 2017, **29**, 1702125.
- 30 W. Zhao, S. Li, H. Yao, S. Zhang, Y. Zhang, B. Yang and J. Hou, J. Am. Chem. Soc., 2017, 139, 7148.
- 31 Y. Yang, Z. G. Zhang, H. Bin, S. Chen, L. Gao, L. Xue, C. Yang and Y. Li, *J. Am. Chem. Soc.*, 2016, **138**, 15011.
- 32 T. Li, Z. Ke, L. Yang, J. Wang, C. Yan, W. Ma and X. Zhan, *Adv. Mater.*, 2017, DOI: 10.1002/adma.201705969.
- 33 Y. Ma, Q. Zheng, L. Wang, D. Cai, C. Tang, M. Wang, Z. Yin and S.-C. Chen, *J. Mater. Chem. A*, 2014, 2, 13905.
- 34 Y. Ma, Q. Zheng, Z. Yin, D. Cai, S.-C. Chen and C. Tang, *Macromolecules*, 2013, 46, 4813.
- 35 I. Osaka, S. Shinamura, T. Abe and K. Takimiya, *J. Mater. Chem. C*, 2013, 1, 1297.
- 36 I. Osaka and K. Takimiya, Adv. Mater., 2017, 29, 1605218.
- 37 I. Osaka, T. Abe, S. Shinamura and K. Takimiya, *J. Am. Chem. Soc.*, 2011, **133**, 6852.
- 38 Y. Yi, H. Feng, M. Chang, H. Zhang, X. Wan, C. Li and Y. Chen, *J. Mater. Chem. A*, 2017, 5, 17204.
- 39 Y. Ma, M. Zhang, Y. Yan, J. Xin, T. Wang, W. Ma, C. Tang and Q. Zheng, *Chem. Mater.*, 2017, 29, 7942.
- 40 S. C. Price, A. C. Stuart, L. Yang, H. Zhou and W. You, *J. Am. Chem. Soc.*, 2011, 133, 4625.
- 41 V. D. Mihailetchi, L. J. Koster, J. C. Hummelen and P. W. Blom, *Phys. Rev. Lett.*, 2004, **93**, 216601.
- 42 I. Riedel, J. Parisi, V. Dyakonov, L. Lutsen, D. Vanderzande and J. C. Hummelen, *Adv. Funct. Mater.*, 2004, **14**, 38.
- 43 A. Hexemer, W. Bras, J. Glossinger, E. Schaible, E. Gann, R. Kirian, A. MacDowell, M. Church, B. Rude and H. Padmore, J. Phys.: Conf. Ser., 2010, 247, 012007.
- 44 E. Gann, A. T. Young, B. A. Collins, H. Yan, J. Nasiatka, H. A. Padmore, H. Ade, A. Hexemer and C. Wang, *Rev. Sci. Instrum.*, 2012, 83, 045110.
- 45 G. G. Malliaras, J. R. Salem, P. J. Brock and C. Scott, *Phys. Rev. B: Condens. Matter Mater. Phys.*, 1998, **58**, 13411.